Received: 22 May 2023 | Accepted: 14 December 2023

DOI: 10.1002/mrd.23725

Molecular Reproduction & Development

RESEARCH ARTICLE

Cystic ovary disease (COD) alters structure and function of the bovine oviduct

Deirdre Scully[1] | Sven Reese[2] | Sabine Kölle[1]

[1]Department of Biomedical Sciences, School of Medicine, Health Sciences Centre, University College Dublin (UCD), Dublin, Ireland

[2]Institute of Anatomy, Histology and Embryology, School of Veterinary Medicine, LMU Munich, Munich, Munich, Germany

Correspondence
Sabine Kölle, Department of Biomedical Sciences, School of Medicine, Health Sciences Centre, University College Dublin, Belfield 18, Dublin 4, Ireland.
Email: sabine.koelle@ucd.ie

Present address
Deirdre Scully, Department of Integrative Physiology, Baylor College of Medicine, Houston, Texas, USA.

Abstract

Cystic ovary disease (COD) is a common cause of subfertility in dairy cattle. Therefore, the aim of this study was to provide novel concepts for cyst classification and to investigate the effects of COD on tubal microarchitecture, oviductal metabolic function, and the formation of the sperm reservoir. Bovine Fallopian tubes affected by follicular cysts, follicular cysts with luteinization and luteal cysts were investigated by a variety of microscopic and histological techniques and compared to control cows in metestrus and diestrus. We defined three types of cysts involved in COD, each of which had a characteristic wall thickness, inner wall appearance and cellular pattern within the cyst aspirate. Regarding the Fallopian tube, each cyst type was associated with a characteristic morphology, specifically the microarchitecture of the folds in ampulla, epithelial cell ratios, and ciliated/secretory cell size and form. Furthermore, each cyst type showed different patterns of tubal glycoprotein and acidic mucopolysaccharide synthesis, which was highly variable as compared to the controls. Our studies are the first to characterize the effects of COD on the Fallopian tube, which promotes the establishment of novel, cyst-specific therapeutic concepts in cattle and helps gain a holistic view of the causes of subfertility in cows with COD.

KEYWORDS

cystic ovary disease, oviduct, sperm reservoir, structure and function

1 | INTRODUCTION

Cystic ovarian disease (COD) is a common disorder leading to reproductive failure in dairy cattle due to an inability of the preovulatory follicle to ovulate. In the bovine, it ultimately leads to significant economic losses due to delays in conception, reduced milk production and treatment costs (Borş & Borş, 2020; Cattaneo et al., 2014). The failure to ovulate is caused by a dysfunction of the hypothalamic-pituitary-gonadal axis as well as intraovarian failures (Noakes et al., 2001; Ortega et al., 2016; Peter, 2004). Bovine COD presents when one or more nonovulatory follicular structures (at least 17 mm in diameter) persist for more than 6 days in the absence of a corpus luteum (CL), thus interrupting ovarian cyclicity (Borş & Borş, 2020; Lüttgenau et al., 2016; Vanholder et al., 2006). Traditionally, bovine ovarian cysts are classified as either follicular cysts (FC) (characterized by high estradiol levels) or luteal cysts (LC) (revealing elevated progesterone secretion) (Noakes et al., 2001; Vanholder et al., 2006). However, there is a third type of cyst, the follicular cyst with luteinization (FCL), which is thought to be in a state of

Summary sentence: COD impairs microarchitecture and function of the bovine oviduct.

transition from follicular to luteal cyst but has not been fully characterized yet (Ortega et al., 2016). For this reason, this type of cyst has been included and discriminated from the other two cysts in this manuscript.

While recent studies have explored the role of the insulin signaling pathway, metabolites and neuropeptides in the pathogenesis of COD (Gareis et al., 2023), its impact on the oviduct is still unknown. The oviduct is essential for gamete transport, formation of the sperm reservoir, fertilization and early embryonic development (Kölle, 2022; Kölle et al., 2020; Suarez, 2008), as well as for the timely transport of the embryo to the uterus for implantation (Dixon et al., 2019). To be able to fulfill all of these functions, the bovine oviduct is divided into four structurally and functionally distinct parts: the infundibulum, ampulla, isthmus and uterine part (Bastos et al., 2022; Fernandez-Fuertes et al., 2018). The infundibulum is located at the ovarian end of the oviduct and exhibits fimbriae which capture the ovulated oocyte and guide it into the ampulla in the bovine (Kölle et al., 2009, 2020). The thin-walled ampulla is highly folded and is not only the site of fertilization, but also the location of the first embryo-maternal communication (Kölle et al., 2009, 2020). At the ampullary-isthmic junction, the ampulla transitions into the thick-walled isthmus which has a pronounced smooth muscle layer. Both in the ampulla and isthmus, spermatozoa form a sperm reservoir by binding with their heads to the ciliated cells (CCs) of the oviductal epithelium (Camara Pirez et al., 2020; Kölle, 2022). This allows spermatozoa to maintain their motility and fertilizing ability until ovulation occurs (Suarez & Pacey, 2006).

The microarchitecture of the oviduct is perfectly adapted to its functions of transport and nutrition. Its inner surface is lined by a pseudostratified columnar epithelium consisting of ciliated and secretory cells (SCs) (Ito et al., 2020, 2023). CCs influence gamete and embryo transport through the oviduct by means of ciliary beating, and nonciliated SCs contribute to the production of oviductal fluid which provides the optimal nutrients and microenvironment for sperm capacitation, fertilization and early embryo survival and development (Croxatto, 2002). In the bovine, the proportion of CCs and SCs change throughout the length of the oviduct and across the estrus cycle, with the number of CCs being increased in the infundibulum and ampulla during the follicular phase of the cycle (Abe & Oikawa, 1993; Ito et al., 2020, 2023). Recently, it has been shown that bovine epithelial remodeling is regulated specifically by SC differentiation/proliferation which implies that CCs in the oviduct may also arise from SCs (Ghosh et al., 2017; Ito et al., 2016, 2020). These changes in the oviductal epithelium are thought to be regulated by estradiol and progesterone.

Overall, the oviduct plays a vital role in gamete transport, gameto-maternal interactions, fertilization, embryonic development and early embryo-maternal communication (Kölle et al., 2020; Kölle, 2022; Suarez, 2008). However, to date, studies investigating the effects of COD on the morphology and function of the oviduct and the resulting implications on fertility are still lacking. The importance of gaining precise insights on the effects of COD on tubal function is highlighted by the fact that after induction of ovulation in COD cows, infertility might persist (Borş & Borş, 2020; Douthwaite & Dobson, 2000). Further to that, cows affected by COD have 4 times less chance of becoming pregnant by the end of lactation than control cows (Cattaneo et al., 2014). These facts point to the necessity of gaining a more comprehensive understanding of this disease in the context of the entire genital tract. Therefore, we set out to characterize alterations in the tubal microarchitecture and metabolic function in cows affected by COD. This study provides a holistic view of the causes of subfertility in cows with COD and emphasizes the requirement for establishing novel, cyst-specific therapeutic concepts in cattle which are aimed at mitigating the effects of COD not only in the ovary, but in all parts of the genital tract.

2 | MATERIALS AND METHODS

2.1 | Ethics

This study did not require ethical approval as bovine tissues were obtained from the abattoir. Full ethical exemption was granted by the Office of Research Ethics, University College Dublin (AREC-E-18-48-KOELLE).

2.2 | Tissue collection

Reproductive tracts from COD cows ($n = 33$) and control cows ($n = 31$) were collected from a local abattoir (Kildare Chilling Company, Kildare, Ireland) as previously described (Scully et al., 2021). Healthy control samples were collected at metestrus (days 1–4) or mid-diestrus (days 11–17). These cycle stages were chosen as control samples because they represent phases of the estrus cycle associated with blood serum levels of estradiol and progesterone comparable to follicular cysts (FC) and luteal cysts (LC) (Brodzki et al., 2019). The cycle stage was determined by gross anatomical inspection of the genital tract as previously described (Scully et al., 2021). Metestrus was characterized by the presence of a recently ovulated point on the external ovarian surface that was red in color (Arosh et al., 2002; Ireland et al., 1980). Mid-diestrus was characterized by the presence of a yellow/orange CL occupying more than 50% of the ovarian surface (Arosh et al., 2002; Ireland et al., 1980). Samples were excluded from the study if there were signs of infection, inflammation or pregnancy. The presence of COD was confirmed if one or both ovaries revealed anovulatory structures greater than 25 mm in diameter in the absence of a CL. FC were determined by a thin wall (0.06 ± 0.01 cm) and a lack of luteinization (absence of yellow/orange coloration on the inner surface). Follicular cysts with luteinization (FCL) also had a thin wall (0.12 ± 0.01 cm) but luteinization was present on the internal cyst wall in isolated patches. LC had a thick wall (0.28 ± 0.03 cm) and at least 50% of the internal cyst wall was luteinized revealing an intense yellow/orange color. Classification of cysts were done by anatomical gross inspection as well as by histomorphological characterization of the cyst wall and the cyst fluid.

2.3 | Oviduct sampling

A total of 1 cm portions of the middle-third of the ampulla were freed from mesosalpinx and placed in phosphate-buffered saline (PBS) (4°C) until further use. Both ipsilateral and contralateral oviducts were collected and processed for experiments. The term ipsilateral refers to the oviduct adjacent to the ovulatory ovary (indicated by a Graafian follicle or CL) or ovary with COD. The term contralateral refers to the oviduct that is on the opposite side of the reproductive tract to ovulation/COD. The ampulla was selected for investigation because this part of the oviduct is the site of sperm binding, fertilization and the first embryo-maternal communication (Kölle et al., 2009, 2020; Kölle, 2022).

2.4 | Collection of cystic fluid

Cystic fluid was aspirated from cysts and processed for histological assessment. Cystic fluid was collected using a syringe and an 18 G needle and the fluid was centrifuged at 200*g* for 5 min (Centrifuge 5702, Eppendorf). The supernatant was removed, the pellet was washed with sterile PBS and centrifuged again. After removal of the supernatant, the pellet was resuspended in 100 µL sterile PBS. A total of 5 µL of this cell suspension (FC: $n = 3$, FCL: $n = 3$, LC: $n = 3$) was dried onto warmed Superfrost Plus slides (Thermo Scientific) and fixed in Bouin's solution (7 min, RT). Slides were washed in PBS (2 × 7 min, RT) and dehydrated in ascending series of ethanols (30%, 50%, 70%, 100%, and 100%; 7 min each, RT) (Honeywell Riedel-de-Haën AG, Seelze). Slides were frozen at −20°C. For hematoxylin staining, specimens were rehydrated in dH_2O (30 s, RT), placed in filtered hematoxylin (VWR, Dublin Ireland; 10 s, RT) and rinsed in PBS (2 × 30 s, RT). Slides were dipped in xylene and cover slipped using DPX (Sigma-Aldrich). Microscopic analyses were performed using an Olympus BX51 microscope equipped with an Olympus DP71 camera (Olympus Corp.).

2.5 | Stereomicroscopic comparison of tubal mucosal surface

Stereomicroscopy was used to qualitatively assess the arrangement and thickness of the folds in the ampullae of mid-diestrus cows (controls: $n = 7$), cows with FC ($n = 7$), FCL ($n = 5$), and LC ($n = 8$). Stereomicroscopy was also used to diagnose the presence of inflammation in the oviduct which is characterized by reddening of the inner surface and clearly marked vessels (Owhor et al., 2019).

A total of 1 cm portions of the ampulla were freed from the mesosalpinx, opened longitudinally, washed with PBS and pinned onto 35 mm petri dishes using the tips of 26 G Sterican® needles (Braun, GmbH). The inner mucosal surfaces of the ampullae were visualized using an Olympus DP-SZX12 microscope (model SZX-ILLK200) and an Olympus DF PLAPO 1× objective (Olympus). For quantitative analysis of oviductal fold thickness, the width of primary folds was measured in three randomly selected areas of interest (AOI) using the line tool in ImageJ® (National Institutes of Health, USA).

2.6 | Preparation of spermatozoa

Frozen bull sperm were obtained from the Irish Cattle Breeding Centre, Kildare, Ireland (breed: Holstein-Friesian; age: 2–3 years, $n = 6$). Only sperm of bulls of proven fertility were used. In each ejaculate used, morphology, motility, viability and sperm membrane integrity before freezing, after freezing and after thawing were examined. Frozen semen was thawed at 39°C for 10 s. The sperm were washed in 1 mL of warm HEPES buffer and centrifuged at 200*g* for 5 min (Centrifuge 5702, Eppendorf). Sperm were then resuspended in 100 µL of warm HEPES buffer. Pre- and postwash sperm motility was assessed using an Olympus phase contrast inverted microscope (Olympus CKX21SF) and a phase contrast lens (Olympus LCAch PHP N 20x/0.4). Only sperm revealing postwash motility of >60% were used for the experiments.

2.7 | Morphological comparison of secretory and CC ratios in the oviductal epithelium

The middle third of the ampulla (1 cm) from control, mid-diestrus cows ($n = 3$) and cows with FC ($n = 3$), FCL ($n = 3$) and LC ($n = 3$) was freed from the mesosalpinx and fixed in Bouin's fixative for 22 h. After washing twice in 70% ethanol and dehydration in ascending series of ethanols (70%, 80%, 90%, 100%, and 100%; 10 min each, RT), specimens were embedded in paraffin. Sections (5 µm) were cut (microtome: Reichert Jung 2030, Leica Microsystems), mounted on Superfrost Plus slides (Thermo Scientific), deparaffinized, hydrated in ascending series of ethanols and stained with hematoxylin and eosin (HE). After staining, specimens were mounted with DPX and cover slipped.

Quantitative analyses of CC and SC ratios were carried out in the ampullae from mid-diestrus cows (control $n = 3$) and COC cows (FC: $n = 3$, FCL: $n = 3$, LC: $n = 3$). Four random AOI were selected per oviduct covering an area of 0.04 mm^2. In each sample 200 cells were counted in total. The following cell types were assessed: CCs, non-protruding secretory cells (non-pSCs), and protruding secretory cells (pSCs). Areas with obliquely cut epithelium were excluded from the analysis. CCs were distinguished by their elongated oval nuclear shape and the basal bodies of the cilia. Non-pSCs were characterized by round nucleus, eosinophilic cytoplasm and an apical surface below the level of the cilia covered with microvilli. PSC's revealed cytoplasmic protrusions, with and without nuclei, bulged above the surface of the epithelium. Cell ratio counts were performed using the Cell Counter plugin in ImageJ® (National Institutes of Health, USA).

2.8 | Histochemical analyses of the synthesis of glycoproteins and acidic mucopolysaccharides

Periodic Acid Schiff (PAS) reaction was used to compare the synthesis of glycogen and glycoproteins in the ampulla from metestrus (control: $n = 3$), mid-diestrus (control: $n = 5$) and COD cows (FC: $n = 9$, FCL: $n = 6$, LC: $n = 10$). After hydration in descending series of ethanols (100%, 90%, 80%, 70%, 10 min each) the sections were placed in 0.5% periodic acid (Sigma-Aldrich; 5 min, RT), followed by running water (10 min), Schiff's reagent (Sigma-Aldrich; 5 min, RT), sulphite water (0.5 g sodium disulfate in 100 mL distilled water; 2 × 3 min) and running water (10 min). After washing in distilled water, hematoxylin (VWR; 30 s) was applied as a counterstain. After dehydration in ascending series of ethanols (70%, 80%, 90%, 100%, and 100%; 10 min each), slides were cover slipped using DPX (Sigma-Aldrich). In a second experiment, glycogen and glycoproteins synthesized in the tubal epithelium were discriminated by digestion of glycogen with 1% Amylase (Sigma-Aldrich; 37°C, 10 min) before placement in 0.5% periodic acid.

Alcian blue (pH 2.5) was applied to compare the localization of acidic mucopolysaccharides in the ampulla from metestrus (control: $n = 5$), mid-diestrus (control: $n = 8$) and COD cows (FC: $n = 9$, FCL: $n = 9$, LC: $n = 14$). Specimens were placed in 3% acetic acid (Sigma-Aldrich; 3 min), followed by 1% Alcian blue in 3% acetic acid (Sigma-Aldrich; pH 2.5, 30 min) and 3% acetic acid (Sigma-Aldrich; 3 min). After washing with distilled water (2 × 3 min), sections were counterstained with 0.1% nuclear Fast Red (Sigma-Aldrich; 3 min). Following dehydration in an ascending series of ethanols (70%, 80%, 90%, 100%, and 100%; 10 min each), sections were cover slipped using DPX (Sigma-Aldrich).

Imaging was performed using an Olympus BX51 microscope (Olympus) and an Olympus DP71 camera (Olympus Corp.).

For glycoprotein and acidic mucopolysaccharide quantification, four random AOI (0.04 mm^2) were selected per oviduct. Each image was converted to an RGB stack in ImageJ® (National Institutes of Health, USA). Using the line selection tool, the epithelium was traced as close to the luminal surface as possible. A plot profile was generated which displayed a 2D profile of the intensities of pixels (0–255) along the line that was drawn. These values were exported to excel and the IF function [IF (x > 100, 0, 1)] was used to calculate the following: If the value of interest is greater than 100 it is assigned "0." "0" = cell not stained with PAS/Alcian blue. If the value of interest is less than 100 it is assigned "1." "1" = cell stained with PAS/Alcian blue. An average was generated to represent the percentage of stained cells in the epithelium analyzed.

2.9 | Scanning electron microscopy (SEM) for comparison of three-dimensional microarchitecture of the tubal mucosa

SEM analyses were carried out for the analysis of the 3D architecture on ampullae from mid-diestrus cows (control: $n = 3$) and ampullae from cows with COD (FC: $n = 6$, FCL: $n = 4$, LC: $n = 8$). Samples were washed in Sorenson's buffer (1:5 solution of 0.07 M KH_2PO_4 and 0.07 M $Na_2HPO_4.2H_2O$, pH 7.4) twice and fixed in 1% glutaraldehyde in Sorenson's buffer (24 h, 4°C). Samples were then dehydrated in series of ascending acetones (10%, 20%, 30%, 40%, 50%, and 60%: 5 min each; 70%, 80%, and 90%: 60 min each; 100% 12 h). Samples were dried at critical point with liquid CO_2 (Union Point Dryer CPD 030, Bal-Tec) and coated with 12 nm gold palladium (Union SCD 040 sputtering device, Bal-Tec). Samples were assessed using a Zeiss scanning electron microscope DSM 950 (Zeiss) at magnifications from ×50 to ×8000.

2.10 | Transmission electron microscopy (TEM) for ultrastructural comparison of tubal cells

TEM analyses were carried out in ampullae from mid-diestrus cows (control: $n = 2$) and ampullae from cows with COD (FC: $n = 1$, FCL: $n = 2$, LC: $n = 3$). 0.5 cm pieces of closed ampulla were fixed in 4% glutaraldehyde in Sorenson's buffer (60 min, 4°C) and were then transferred to 2.5% glutaraldehyde solution in Sorenson's buffer (2 h, 4°C). After washing in cacodylic acid buffer (0.1 M $C_2H_7AsO_2$, 3 × 5 min) specimens were contrasted with osmium tetroxide potassium ferrocyanide (O_5O_4-$K_4Fe(CN)_6.[Fe(CN_6)]_4$; 4 h, RT). Samples were washed again in cacodylic acid buffer (3 × 5 min) and were dehydrated in ascending series of ethanols (70%, 80%, 90%, 100%, and 100%; 2 × 15 min each). Samples were placed in a solution of propylene oxide (C_3H_6O): epoxy resin at a ratio of 1:2 (60 min), followed by a 1:1 ratio solution of propylene oxide (C_3H_6O): epoxy resin (12 h) and a 2:1 ratio solution of propylene oxide (C_3H_6O): epoxy resin (60 min) and finally in pure epoxy resin. Semithin sections (0.5 µm) were cut for initial evaluation and stained with methylene blue. After selecting the best regions in semithin sections, ultrathin sections (90 nm) were cut and placed on copper grids. These sections were contrasted for viewing with a saturated solution of uranyl acetate ($UO_2(CH_3COO)_2.2H_2O$; 10 min). Sections were washed briefly in dH_2O, dried and examined using a Zeiss EM 9 microscope with points electronics digital upgrade (magnifications of ×5000 to ×30,000) and equipped with a slow scan CCD camera 7899 (TRS). Panorama views of up to 50 cells were created using Image SP 1.2.8.111 (Sys Prog).

2.11 | Quantitative analyses of sperm motility and sperm survival time in the tubal sperm reservoir using digital live cell imaging

For digital live cell imaging, samples of ampulla (1 cm) were freed from mesosalpinx, opened longitudinally, and pinned onto Delta T dishes (Bioptech Inc.) precoated with a 2 mm layer of silicone (Sylgard® 184, Dow Corning). Samples were washed with PBS followed by HEPES buffer (10 mM HEPES, 136.4 mM NaCL, 5.6 mM KCL, 2.2 mM $CaCL_2.2H_2O$, 1 mM $MgCl_2.6H_2O$, and 11 mM glucose) and then incubated with HEPES buffer in a humidified chamber for 10 min. Once mounted, samples were maintained at 37.5°C ± 1 using

a stage heater (Delta T Controller, Bioptech Inc.) and an objective heater (Delta T Controller, Bioptech Inc.). The reference temperature of media in the Delta T dish was monitored before all recordings. Imaging was performed with a fixed-stage, upright Olympus microscope (BX51WI) with water immersion objectives equipped with the bright-field long-distance immersion objectives UMPLFLN 10Xw, UMPLFLN 20Xw, and UMPLFLN 40xW (Olympus). Images and videos were documented with a SUMIX Mx7 camera (Sumix).

Overall, sperm motility within the sperm reservoir in the ampulla was assessed in mid-diestrus (control $n = 4$) and COD cows (FC $n = 3$, LC $n = 4$) cows. 1 cm samples of ampulla were prepared for live cell imaging as previously described and incubated with 20 µL of sperm (approximately 600,000 sperm) for 10 min at 37°C. The formation of the sperm reservoir was recorded using the software StreamPix® 7.0 (NorPix) linked to a SUMIX Mx7 camera (100 frames per second). For each specimen, five ROIs with sperm binding were randomly selected and recorded for 15 min. The total number of motile, immotile and hyperactivated sperm was assessed using ImageJ® (National Institutes of Health, USA) software and calculated as a percentage of the total number of bound sperm.

2.12 | Statistical analyses

All statistical analyses were performed using SPSS (Version 27, 2022) and Graph Pad Prism software. For all data, the normality of the distribution was checked using the Shapiro–Wilk test. Normally distributed data were presented as the mean values ± *SEM*. The Chi-square test for trend was used to assess correlation for the presence of inflammation and COD and secretory plasma membrane opening in bulging tubal cells. In the bovine ampulla, an analysis of variance (ANOVA) test with a Dunnett's post hoc test was used to compare epithelial cell ratio in cows with COD and controls. Levene's test for equality of variances was used to compare the mean coefficient of variation of glycogen and acidic mucopolysaccharide synthesis in control cows and cows with COD. Differences were considered statistically significant if $^{*}p \leq 0.05$, $^{**}p \leq 0.01$, and $^{***}p \leq 0.001$.

3 | RESULTS

3.1 | Incidence and classification of cystic ovary disease (COD) in slaughtered cows in Ireland

To assess the incidence of COD, postmortem examinations were carried out on 453 female reproductive tracts from cattle slaughtered during a 21-month period in an Irish abattoir. During this period, the incidence of COD was found to be 3.1%.

Over a 48-month period, 55 tracts affected by COD were investigated, of which 38%, 18%, and 44% presented with FC, FCL, and LC, respectively. FC had a thin wall and did not reveal any signs of luteinization (Figure 1a). FCL showed luteinization in spots (Figure 1b, arrow) or isolated patches (Figure 1b, asterisk). LC were identified when more than half of the cyst wall showed complete and evenly distributed luteinization (Figure 1c, arrow). The cyst wall was significantly thicker in LC ($n = 7$) as compared to FCL ($n = 5$) ($p = 0.003$, Unpaired the Student *t*-test) (Figure 1g). As shown by histological analyses, this was due to the increased size of luteinized cells and increased thickness of underlying connective tissue in the cyst wall.

Aspirates from FC were clear and yellowish in color with a finely granular background. Granulosa cells were abundant and were arranged in clusters (Figure 1d, thick arrow) or in isolation (Figure 1e, thin arrow). Intact granulosa cells were round or oval in shape, with coarsely granular cell nuclei, and a small rim of distinct basophilic cytoplasm (Figure 1d, #1). Follicular cyst aspirates contained apoptotic granulosa cells undergoing nuclear shrinkage (pyknosis) (Figure 1d, #2), as well nuclear fading (karyolysis) or fragmentation (karyorrhexis) (Figure 1d, #3). The aspirates from FCL and LC were yellow to brownish in color, often with a hemorrhagic background and distinct fibrin threads. FCL aspirates contained large granulosa cells. Their nuclei showed coarsely granular chromatin and their cytoplasm was foamy and micro-vacuolated, indicative of the beginning of luteinization (Figure 1e, #4). Aspirates from FCL and LC contained lutein cells which were round with distinct borders. Lutein cells had round, small and eccentric nuclei, as well as abundant basophilic cytoplasm with micro-vacuoles (Figure 1e,f, #5). Degenerating lutein cells were present undergoing pyknosis (Figure 1e,f, #6) and karyorrhexis/karyolysis (Figure 1e,f, #7). LC aspirates also showed evidence of binucleated lutein cells (Figure 1f, #8).

Overall, with progressing luteinization, the number of granulosa cells decreased while the number of lutein cells increased, forming clusters (Figure 1f, top right).

3.2 | COD more commonly affects the right ovary and is more likely to be affected by endometritis

Macroscopic anatomical assessments revealed that of the 31 control (estrus, metestrus, diestrus, proestrus) reproductive tracts investigated (Figure 2a) the frequencies of ovulation from left (52%) and right (48%) ovaries were similar ($p = 0.14$, Binomial test) (Figure 2e). Cysts were more common on the right ovary in reproductive tracts with COD, specifically in tracts with LC ($p = 0.01$, Binomial test) (Figure 2b and 2e, R: right, L: left).

Reproductive tracts with FC, FCL, and LC were significantly more likely to reveal endometritis (characterized by reddish color of the mucosa and accumulation of secretions, Figure 2d) than control cows with a regular pink inner surface (Figure 2c) ($p = 0.019$, $p = 0.029$, $p = 0.017$ respectively, Pearson-Mantel-Haenszel's Chi-square test) (Figure 2f).

3.3 | COD is correlated with increased thickness of mucosal folds and fold fusion

The 3D tubal microarchitecture was assessed using SEM. Ampullae from control, mid-diestrus cows showed longitudinally

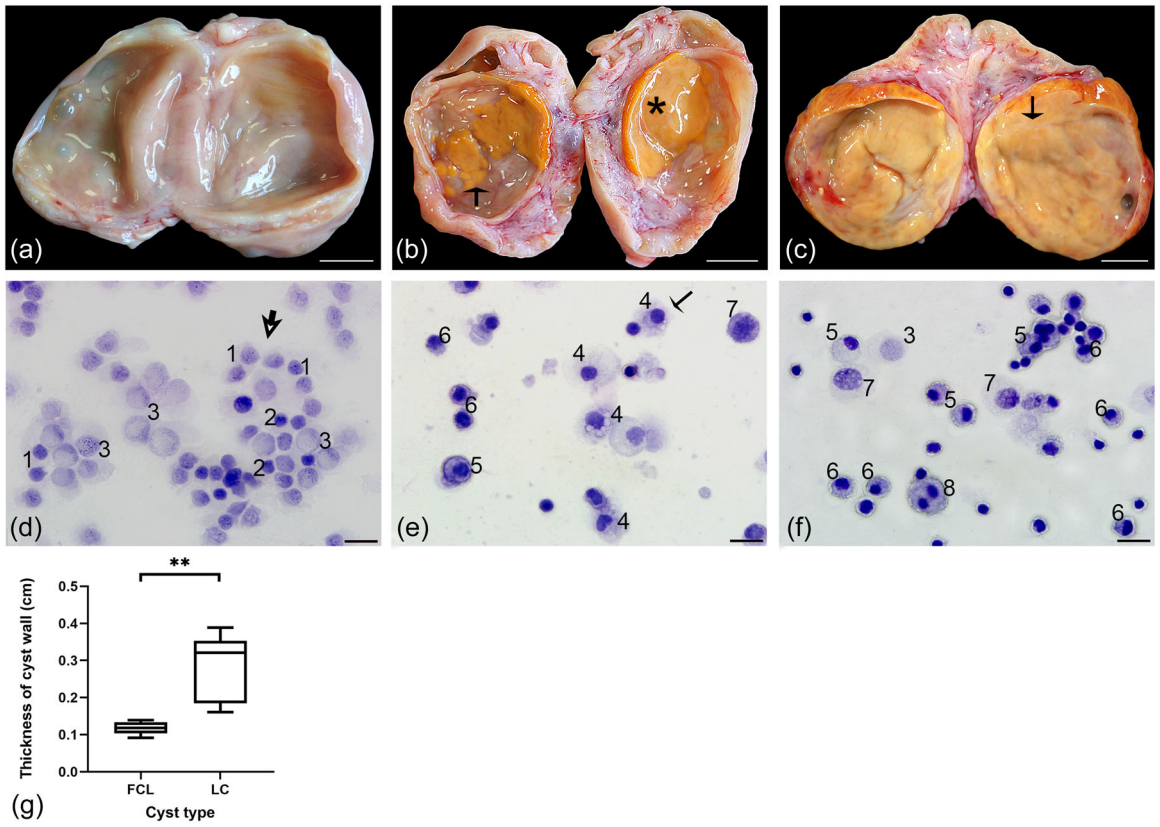

FIGURE 1 Classification of cystic ovary disease (COD) in slaughtered cows. (a) Follicular cyst (FC). (b) Follicular cyst with luteinization (FCL). Luteinization is visible in the form of spots (arrow) or of isolated patches (asterisk). (c) Luteal cyst (LC). Luteal tissue covers most of the inner surface area (arrow). (d–f) Cytology of cyst aspirates. (d) Aspirates from FC reveal intact granulosa cells (1); granulosa cells with pycnotic nuclei (2); granulosa cells with karyorrhexis/karyolysis (3). Granulosa cells are often arranged in clusters (thick arrow). (e) Aspirates from FCL show granulosa cells with luteinization (4); lutein cells (5); lutein cells with pyknotic nuclei (6); and lutein cells with karyorrhexis/karyolysis (7). Cells in the aspirate mostly occur as single cells (thin arrow). (f) Aspirates from LC reveal granulosa cells with karyorrhexis/karyolysis (3); lutein cells (5); lutein cells with pyknotic nuclei (6); lutein cells with karyorrhexis/karyolysis (7) as well as lutein cells with binucleation (8). (g) The cyst wall is significantly thicker in LC than in FCL ($p = 0.003$, unpaired the Student t-test). Scale bars a–c: 1 cm; d–f: 20 µm.

orientated primary folds (Figure 3a, **A**) which gave rise to secondary (Figure 3a, **B**) and tertiary (Figure 3a, **C**) folds. Secondary and tertiary folds branched towards basal areas between folds which showed a strong degree of organization as a net of oval shaped pockets (Figure 3a, asterix). In all cows with cysts, primary and secondary tubal folds were irregular in form and size due to fold fusion. The highest degree of irregularity and fold fusion was seen in oviducts from LC cows (Figure 3b–d). As a consequence, the basal areas (pockets) between the folds were hidden in ampullae from cows with FC (Figure 3b), FCL (Figure 3c), and LC (Figure 3d).

Using stereomicroscopy, the thickness of the primary folds was compared quantitatively. The results showed that longitudinally orientated primary folds were thicker in the ampulla from cows with FC (1.5 ± 0.1 mm, $n = 7$), FCL (1.2 ± 0.1 mm, $n = 5$) and LC (1.3 ± 0.1 mm, $n = 8$), as compared to controls (1.1 ± 0.1 mm, $n = 7$). Mucosal fold thickness was significantly increased in the FC group compared to the control group ($p = 0.02$, ANOVA with Dunnett's) (Figure 3e).

3.4 | COD increases the abundance of SCs

HE staining and histomorphological quantitative analyses were performed to evaluate the effect of COD on the occurrence of epithelial cell types. Figure 4 illustrates the typical cells of the oviductal epithelium: CCs (thick arrow), non-pSCs (thin arrow) and pSCs with apical cytoplasmic protrusions (arrow). Semi-quantitative analyses of the epithelial cells (areas: 0.04 mm^2) demonstrated that non-pSCs were significantly increased in ampullae from FC (Figure 4b, $n = 3$) and FCL (Figure 4c, $n = 3$) cows as compared to control, mid-diestrus cows (Figure 4a, $n = 3$) ($p = 0.001$ and $p = 0.0005$, respectively, ANOVA with Dunnett's) (Figure 4e). The percentage of pSC (Figure 4a–c), was significantly decreased in FC and FCL cows as compared to the controls ($p = 0.003$ and $p = 0.01$, respectively, ANOVA with Dunnett's) (Figure 4f).

The proportion of protruding and nonprotruding SC in ampullae from cows with LC (Figure 4d, $n = 3$) was similar to controls ($p = 0.3$ and $p = 0.14$ respectively, ANOVA with Dunnett's). When comparing proportions of CCs, all groups were similar ($p = 0.17$, ANOVA with Dunnett's).

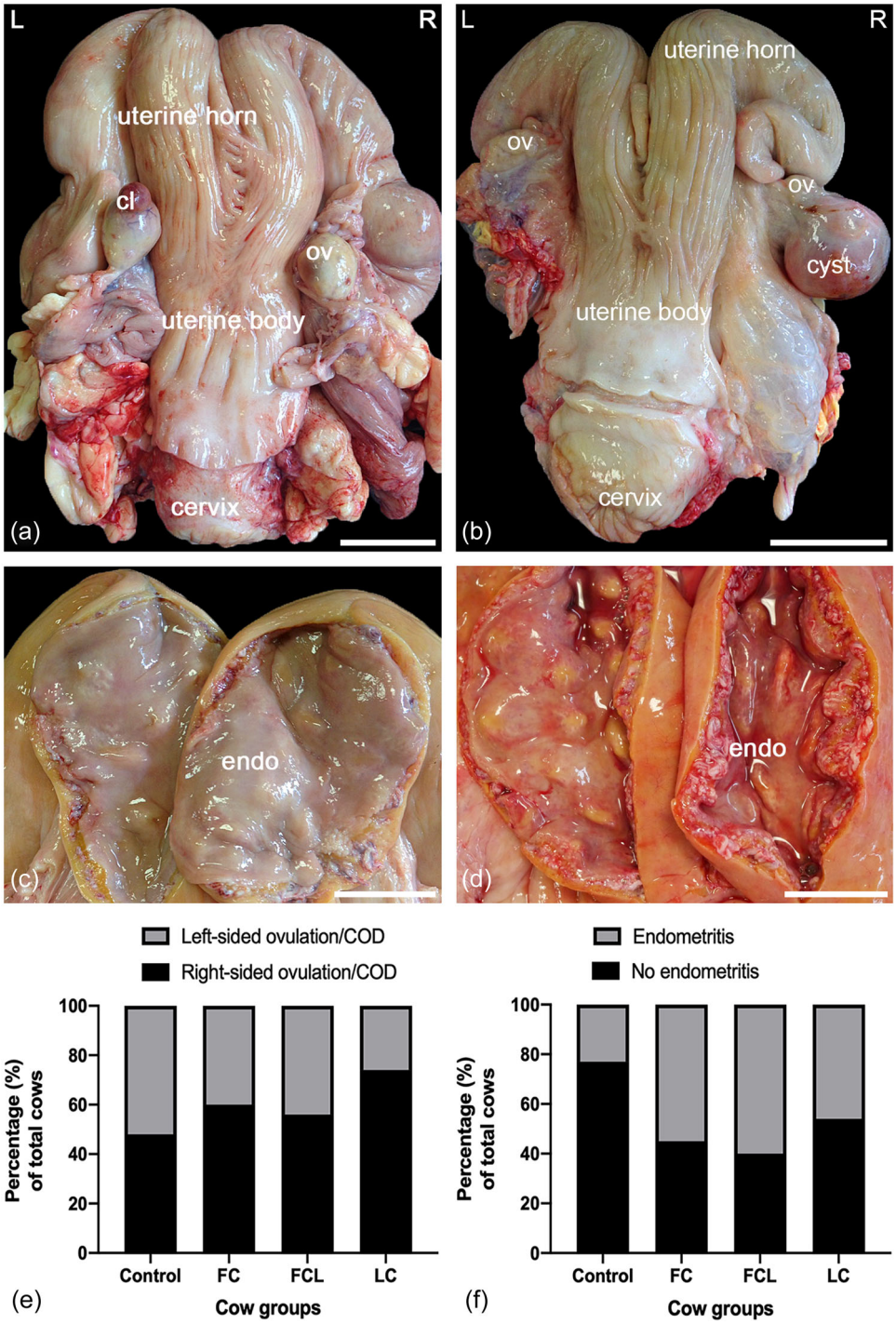

FIGURE 2 Localization of cystic ovary disease (COD) and co-incidence of COD and endometritis. (a) Reproductive tract from a healthy control cow in diestrus. A corpus luteum (CL) is visible on the left (L) ovary (ov). (b) Reproductive tract from a cow with COD. A luteal cyst is visible on the right (R) ovary (ov). (c) Reproductive tract without endometritis. (d) Reproductive tract with endometritis characterized by accumulations of secretions and the reddish color of the inner surface of the endometrium (endo). (e) The percentage of right- and left-sided ovulations is similar in control cows. However, in cows with ovarian cysts [follicular cyst (FC); follicular cyst with luteinization (FCL); luteal cyst (LC)], right-sided cysts are more common than left-sided cysts, which is most distinct in cows with LC ($p = 0.01$, binomial test). (f) Cows with FC, FCL, and LC are more likely to reveal endometritis than control cows. Scale bars: 2 cm.

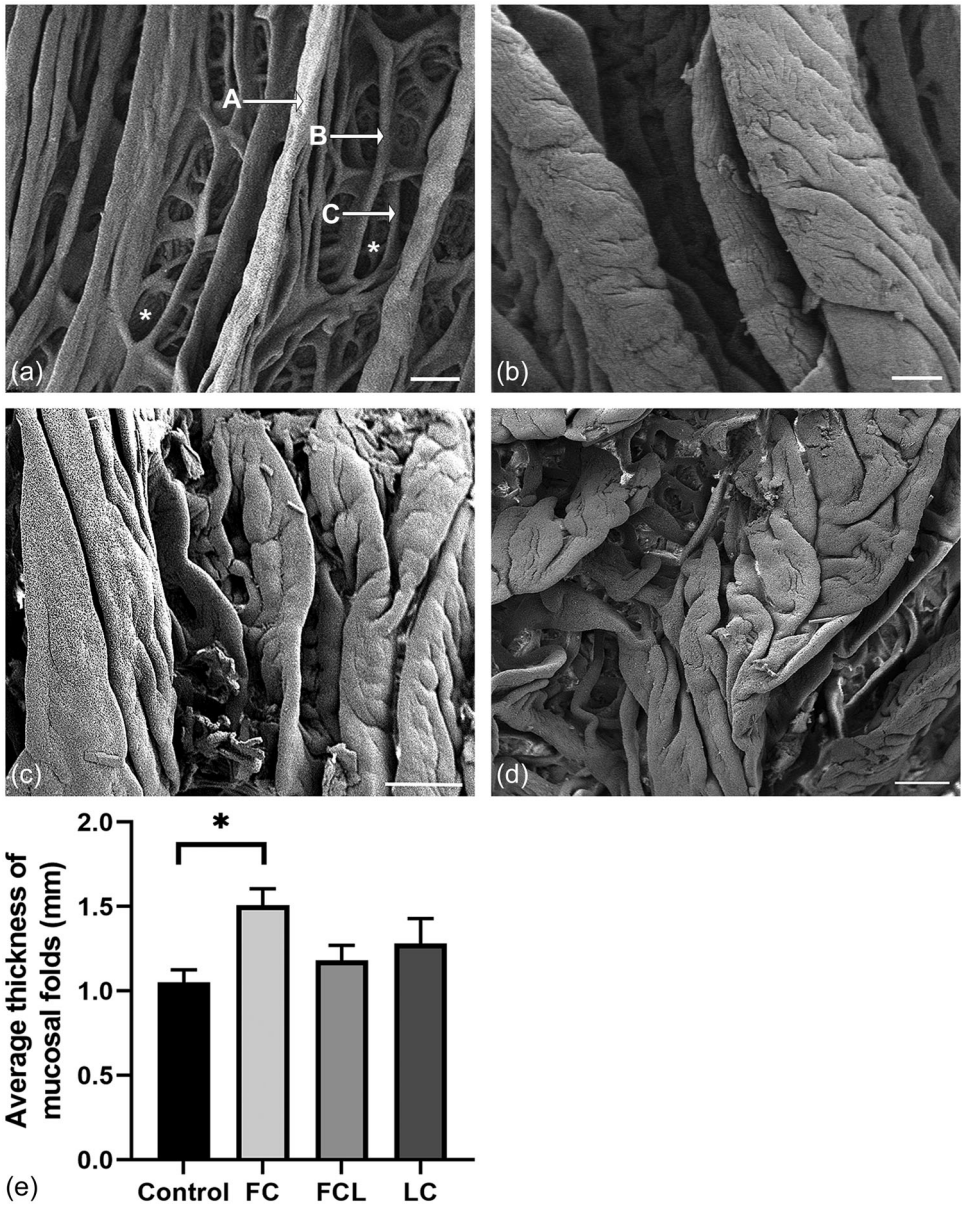

FIGURE 3 Microarchitecture of the oviductal inner surface as seen by scanning electron microscopy (SEM). (a) The ampulla from control cows in mid-diestrus reveals primary (a), secondary (b), and tertiary (c) folds with oval shaped pockets in basal areas between folds (asterisk). Contrary, the tubal mucosa from (b) cows with FC, (c) cows with FCL and (d) cows with LC exhibit thick and fused folds which obscure the basal areas (pockets) between folds. (e) Primary folds in ampullae from FC cows are significantly thicker than primary folds in control cows ($p = 0.02$, ANOVA with Dunnett's). Data are presented as mean ± *SEM*. Scale bars: 500 µm.

3.5 | COD alters epithelial microarchitecture in the ampulla

Oviductal cellular microarchitecture and ratios of secretory and CCs were compared using SEM. Confirming the histological findings, the epithelium of the control ampulla ($n = 3$) was dominated by pSCs, which exhibited bulbous processes that extended to the level of the cilia and beyond (Figure 5a, arrows). In contrast, the ampullae from cows with FC ($n = 6$) predominantly revealed non-pSCs which were gently rounded at the apical surface (Figure 5b, arrowhead). Ampullae from cows with FCL ($n = 4$) contained both nonprotruding (Figure 5c, arrowhead) and protruding SCs (Figure 5c, arrow). However, the apical surfaces of these cells rarely extended to the level of the cilia and were abundantly covered with microvilli. Similar to the control cows in mid-diestrus, pSCs were a predominant feature of the ampullar epithelium in LC cows ($n = 8$) (Figure 5d, arrow). In cows with LC, these pSCs also showed distinct openings in the plasma membrane (Figure 5e, thick arrows), indicating active and recent secretion. Quantitative analyses confirmed that the number of plasma membrane openings was significantly increased in ampullae from cows with LC ($p < 0.0001$, Chi-square test) (Figure 5f).

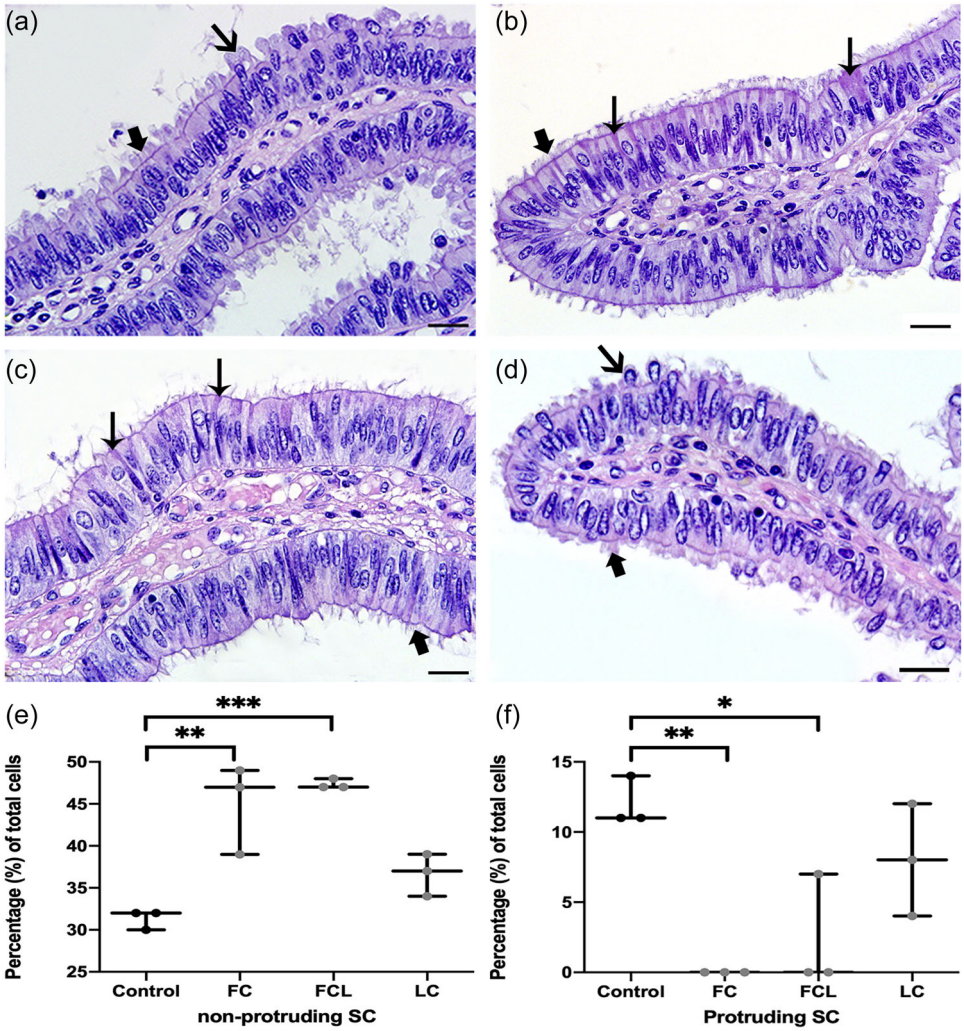

FIGURE 4 Effect of COD on the histomorphology of the bovine ampulla. The tubal epithelium from (a) control, mid-diestrus cows, (b) cows with FC, (c) cows with FCL and (d) cows with LC reveal ciliated cells (thick arrow), nonprotruding secretory cells (thin arrow) and protruding secretory cells (arrow). (e) The percentage of nonprotruding secretory cells (SC) is significantly increased in the ampullar epithelium from cows with FC and FCL compared to control cows ($p = 0.001$ and $p = 0.0005$, respectively, ANOVA with Dunnett's). (f) Contrary, the percentage of protruding SC is significantly decreased in the ampullar epithelium from cows with FC and FCL as compared to control cows ($p = 0.003$ and $p = 0.01$, respectively, ANOVA with Dunnett's). Significance: $^{*}p < 0.05$; $^{**}p < 0.01$; $^{***}p < 0.001$. Data are presented as mean ± *SEM*. Scale bars: 20 µm. ANOVA, analysis of variance; COD, cystic ovary disease; FC, follicular cysts; FCL, follicular cysts with luteinization.

3.6 | COD increases tubal epithelial secretory activity

Epithelial ultrastructure was assessed using TEM. The tubal epithelium from control, mid-diestrus cows (Figure 6a), cows with FC (Figure 6b), cows with FCL (Figure 6c), and cows with LC (Figure 6d) revealed columnar CCs with cilia (Ci), non-pSCs, often covered by microvilli (MV), as well as pSCs (PC) which were or were not covered by microvilli. These cells were connected by desmosomes (D). In control cows, all cell types revealed high amounts of mitochondria (M) and rough endoplasmic reticulum (rER) with ribosomes (R) (Figure 6a). SCs showed a moderate number of secretory granules (SG) in their cytoplasm (Figure 6a). In comparison, the tubal epithelium from cows with ovarian cysts was characterized by the presence of highly active, dilated rER (drER) as well as enlarged mitochondria (EM) characterized by a partial loss of cristae. High amounts of SG were visible in the cytoplasm, which had either electron dense or electron lucent contents.

3.7 | COD increases the ampullar synthesis of glycoproteins

Glycoprotein synthesis was analyzed using the PAS reaction in ampullae from control metestrus ($n = 3$) and mid-diestrus cows (Figure 7a, $n = 5$) as well as cows with FC (Figure 7b, $n = 9$), FCL (Figure 7c, $n = 6$) and LC (Figure 7d, $n = 10$). Both cows in metestrus and mid-diestrus were included as controls as glycoprotein synthesis

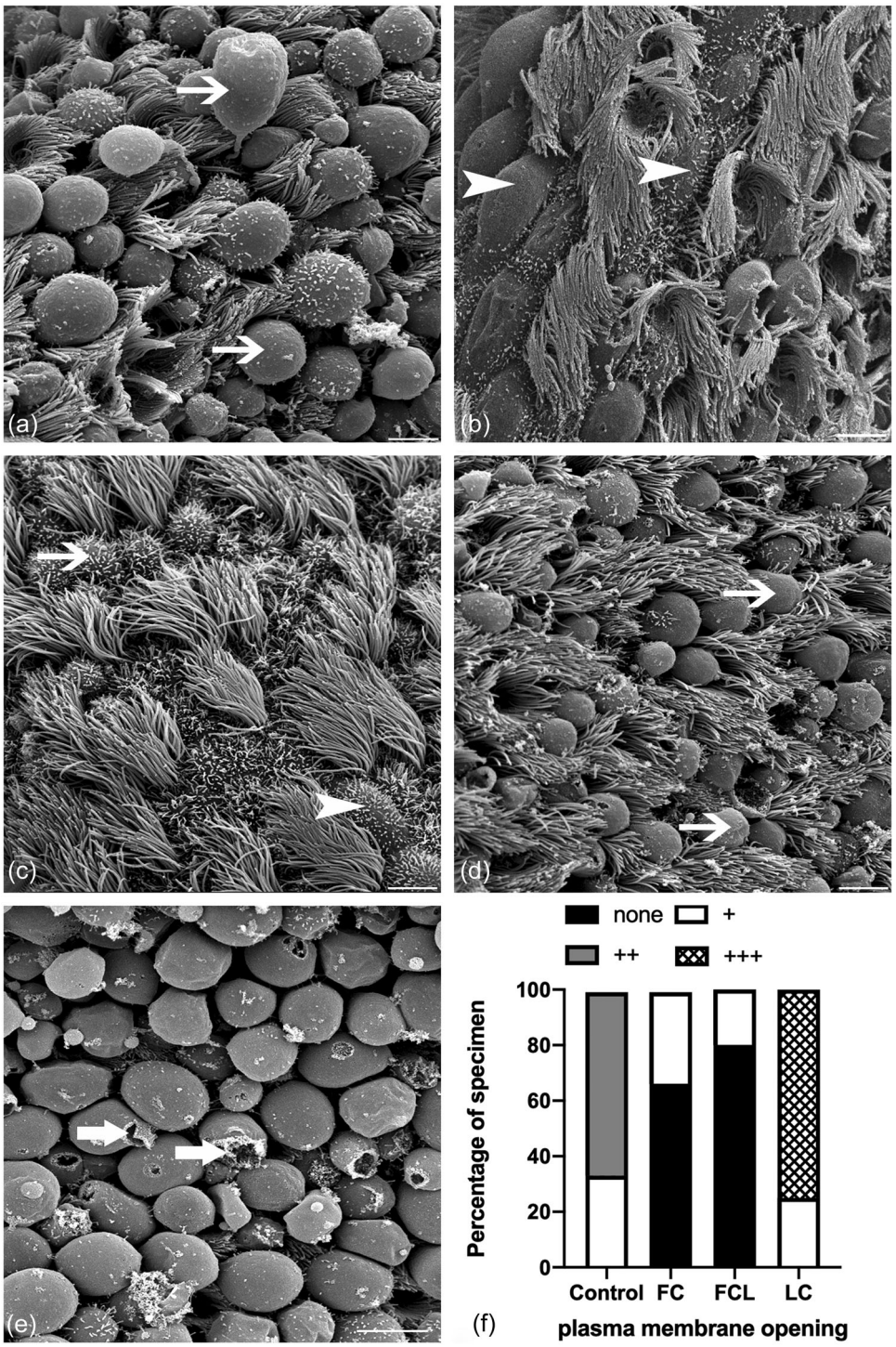

FIGURE 5 Effect of COD on the microarchitecture of the inner surface in the bovine ampulla. The tubal epithelium from (a) control, mid-diestrus cows, (b) cows with FC, (c) cows with FCL and (d) cows with LC reveal secretory cells that are protruding (arrows) and nonprotruding (arrowheads). (e) Openings in the plasma membrane of secretory cells (thick arrows) are indicate active secretion. (f) Plasma membrane openings are significantly increased in cows with LC ($p < 0.0001$, Chi-Square test). Scale bars: 5 µm. COD, cystic ovary disease; FC, follicular cysts; FCL, follicular cysts with luteinization.

is known to vary during the cycle due to changing hormone levels. Glycoproteins were localized in the apical parts of non-pSCs (Figure 7b,c, arrow) as well as in peg cells (Figure 7a and 7d, arrowhead) and along the apical epithelial membrane (Figure 7a and 7d, thick arrow). Glycoprotein synthesis was significantly increased in the ampulla from cows with FC as compared to control cows in metestrus and mid-diestrus ($p = 0.03$ and $p = 0.0008$ respectively, ANOVA with Tukey's) (Figure 7e). Glycoprotein synthesis was also significantly increased in ampullae from cows with FCL as compared to control cows in mid-diestrus ($p = 0.0058$, ANOVA with

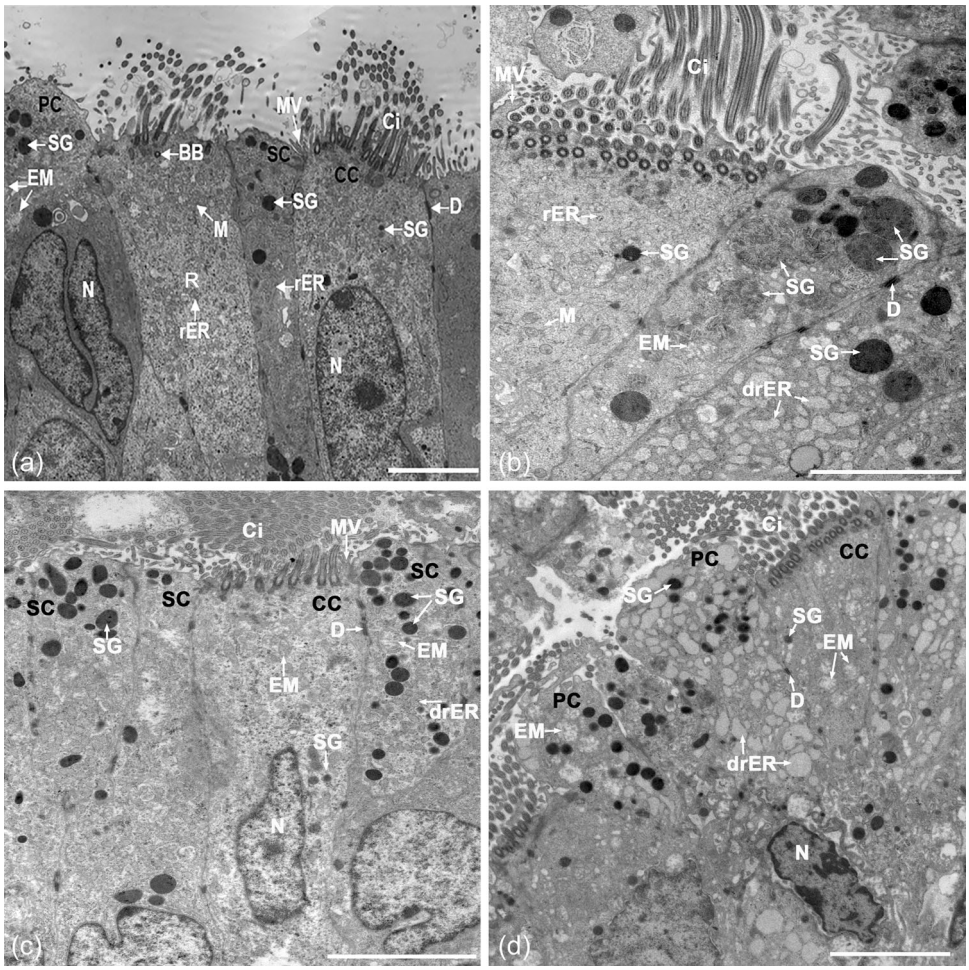

FIGURE 6 Effect of COD on the epithelial ultrastructure in the bovine ampulla. The tubal epithelium from (a) control, mid-diestrus cows (b) cows with FC, (c) cows with FCL and (d) cows with LC reveals ciliated cells (CC) with cilia (Ci), nonprotruding columnar secretory cells (SC) with microvilli (MV), as well as protruding secretory cells (PC). Cells are connected by desmosomes (D). In control cows, all cell types reveal mitochondria (M) and rough endoplasmic reticulum (rER) with ribosomes (R). Secretory cells (SC) have secretory granules in their cytoplasm (SG). Contrary, the tubal epithelium from cows with cysts have dilated rER (drER), enlarged mitochondria (EM) and secretory granules (SG). Scale bars: a = 10 µm, b = 5 µm. COD, cystic ovary disease.

Tukey's), but not in cows with LC ($p = 0.15$, ANOVA with Tukey's) (Figure 7e). However, when comparing the mean coefficient of variation of glycoprotein synthesis in ampullae from control cows with that of cows affected by FC, FCL, and LC, there was a significant increase in ampullae from cows with FCL and LC ($p = 0.016$ and $p = 0.031$, respectively, Levene's test for equality of variances).

3.8 | COD alters the synthesis of acidic mucopolysaccharides in the ampulla

Acidic mucopolysaccharide synthesis was analyzed using the Alcian Blue reaction (pH 2.5) in ampullae from control metestrus ($n = 5$) and mid-diestrus cows (Figure 8a, $n = 8$) as well as from cows with FC (Figure 8b, $n = 9$), FCL (Figure 8c, $n = 9$) and LC (Figure 8d, $n = 14$). Acidic mucopolysaccharides were localized in the apical cytoplasm of non-pSCs (Figure 8b,c, arrows) as well as in peg cells (Figure 8a and 8d, arrowheads) and along the apical epithelial membrane (Figure 8a and 8d, thick arrows). Acidic mucopolysaccharide synthesis was significantly increased in the ampulla from cows with FC as compared to control cows in metestus and mid-diestrus ($p = 0.018$ and $p = 0.0001$, respectively, ANOVA with Tukey's) (Figure 8e). Acidic mucopolysaccharide synthesis was also significantly increased in ampullae from cows with FCL as compared to control cows in mid-diestrus ($p = 0.005$, ANOVA with Tukey's). However, the amount of acidic mucopolysaccharides in cows with LC was similar to controls ($p = 0.336$, ANOVA with Tukey's) (Figure 8e). When comparing the mean coefficient of variation of acidic mucopolysaccharide synthesis in ampullae from control cows (metestrus and mid-diestrus) with that of cows affected by FC, FCL and LC, there was a significant increase in variation in ampullae from cows with FCL and LC ($p = 0.004$ and $p = 0.021$, respectively, Levene's test for equality of variances).

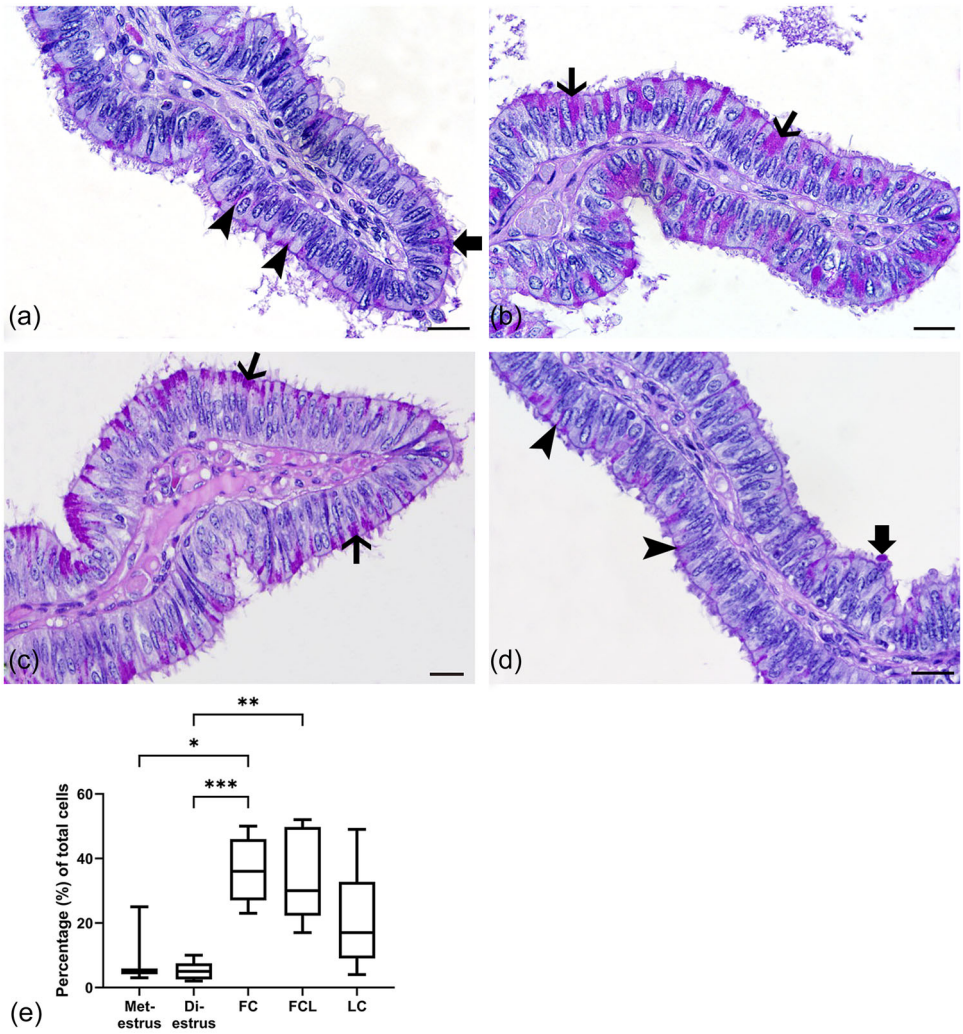

FIGURE 7 The effect of COD on glycoprotein synthesis in the bovine ampulla. The tubal epithelium from (a) control, mid-diestrus cows, (b) cows with FC, (c) cows with FCL, and (d) cows with LC reveals glycoprotein synthesis in peg cells (arrowheads) and in the cytoplasm of nonprotruding SC (arrows). Accumulations of glycoproteins are seen in at the plasma membrane of ciliated and secretory cells (thick arrow). (e) Glycoprotein synthesis was significantly increased in the ampulla from cows with FC as compared to control cows in metestrus and mid-diestrus ($p = 0.03$ and $p = 0.0008$, respectively, ANOVA with Tukey's) as well as in FCL cows as compared to mid-diestrus controls ($p = 0.0058$, ANOVA with Tukey's). Significance: $^{*}p < 0.05$; $^{**}p < 0.01$, $^{***}p < 0.001$. Data are presented as mean ± *SEM*. Scale bars: 20 µm. ANOVA, analysis of variance; COD, cystic ovary disease; FC, follicular cysts; FCL, follicular cysts with luteinization.

3.9 | The formation of the sperm reservoir as well as sperm motility and sperm survival time are maintained in COD

As seen by live cell imaging within the oviduct, sperm formed a sperm reservoir by binding to the CCs of the control ampulla and the ampulla from cows with FC, FCL, and LC in the same manner, at a tangential angle of about 30 degrees (Figure 9a; see Movie S1). In all groups, bound sperm exhibited different patterns of motility which were classified as motile, immotile or hyperactivated (control: Figure 9b, $n = 4$), (FC: Figure 9c, $n = 3$), (LC: Figure 9d, $n = 4$). Motile sperm were characterized by low amplitude, symmetrical flagellar beating (Figure 9b–d, arrow; see Movie S1), while immotile sperm were characterized by a straight, nonbeating flagellum (Figure 9b–d, arrowhead; see Movie S1). Hyperactivated sperm were characterized by a high-amplitude, asymmetrical flagellar beating (Figure 9b–d inlay, arrow; see Movie S2). As there were no differences between FCL and LC cows further statistical analyses focused on comparing FC and LC cows to control cows. The total number of bound sperm per 0.02 mm^2 in the control ampulla was 13 ± 1.6. The total number of bound sperm was similar in ampullae from cows with FC (12 ± 2.2) and LC (12 ± 1.4) ($p = 0.93$ and $p = 0.87$ respectively, ANOVA with Dunnett's). The percentage of motile, immotile and hyperactivated sperm in the control ampulla was 80.5% ± 3.2%, 16.26% ± 4.7%, and 3.29% ± 1.6%, respectively. Overall, the percentage of motile, immotile, and hyperactivated sperm did not significantly differ in ampullae from cows with FC and LC ($p = 0.14$, two-way ANOVA with Tukey's multiple comparisons test) (Figure 9e).

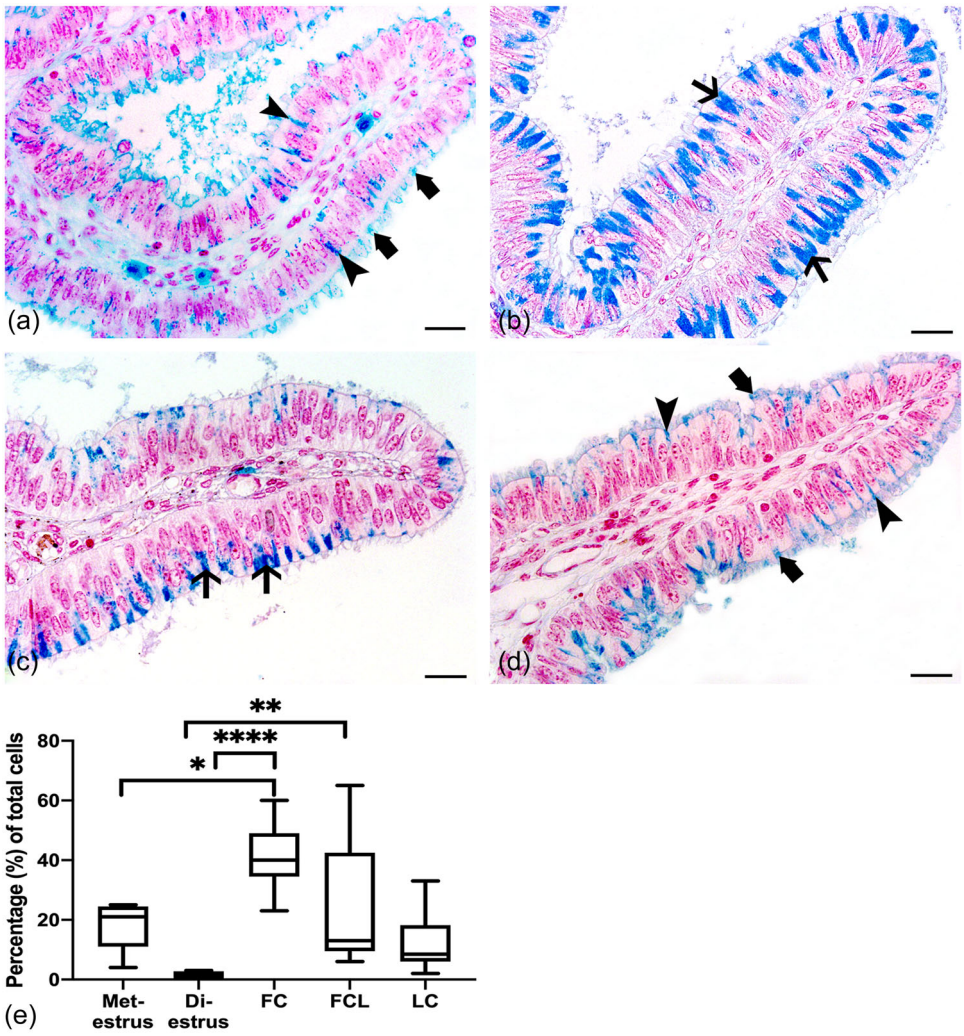

FIGURE 8 The effect of COD on the synthesis of acidic mucopolysaccharides in the bovine ampulla. The tubal epithelium from (a) control, mid-diestrus cows, (b) cows with FC, (c) cows with FCL, and (d) cows with LC show the presence of acidic mucopolysaccharide in peg cells (arrowheads), in the cytoplasm of nonprotruding SC (arrows), as well as at the apical epithelial plasma membrane (thick arrows). (e) Acidic mucopolysaccharide synthesis was significantly increased in the ampulla from cows with FC as compared to control cows in metestus and mid-diestrus ($p = 0.018$ and $p = 0.0001$, respectively, ANOVA with Tukey's) as well as in FCL cows as compared to mid-diestrus controls ($p = 0.005$, ANOVA with Tukey's). Significance: $^{*}p < 0.05$; $^{**}p < 0.01$; $^{***}p < 0.001$; $^{****}p < 0.0001$. Data are presented as mean ± *SEM*. Scale bars: 20 µm. ANOVA, analysis of variance; COD, cystic ovary disease; FC, follicular cysts; FCL, follicular cysts with luteinization.

4 | DISCUSSION

This study is the first to elucidate the impact of COD on the microarchitecture and function of the oviduct, which is the site of formation of the sperm reservoir, fertilization and early embryonic development and plays a key role in fertility (Kölle et al., 2009, 2020; Kölle, 2022). Our previous studies (Scully et al., 2021) have already shown that COD impacts the transport function of the oviduct, highlighting the importance of investigating the effects of COD on all reproductive organs in addition to the existing studies of the ovarian anatomical features associated with COD and its effects on ovarian function (Borş & Borş, 2020; Gareis et al., 2023). Overall, it is important to highlight that bovine COD more often affects the right ovary pointing to different follicular and luteal dynamics in the right and left ovary. This might be related to differences in the inherent intraovarian angio-architecture (Ginther, 2020a). Similarly, in heifers, it has been reported that ovulation is more likely to occur from the right ovary (Ginther, 2020b). Contrary, this is not seen in the adult cows in our studies highlighting the impact of age on ovarian dynamics.

In regard to the **effects of COD on the microarchitecture** of the Fallopian tube, each ovarian cyst type is associated with a characteristic morphology of the inner tubal surface. This includes the 3D microarchitecture of the tubal folds in the ampulla, as well as the cell ratio, and the form and size of the CCs and SCs in the oviductal epithelium. In regard to the tubal folds, the most distinct effect of COD is the fusion of primary and secondary folds. This fusion results in a reduction of the inner luminal surface and

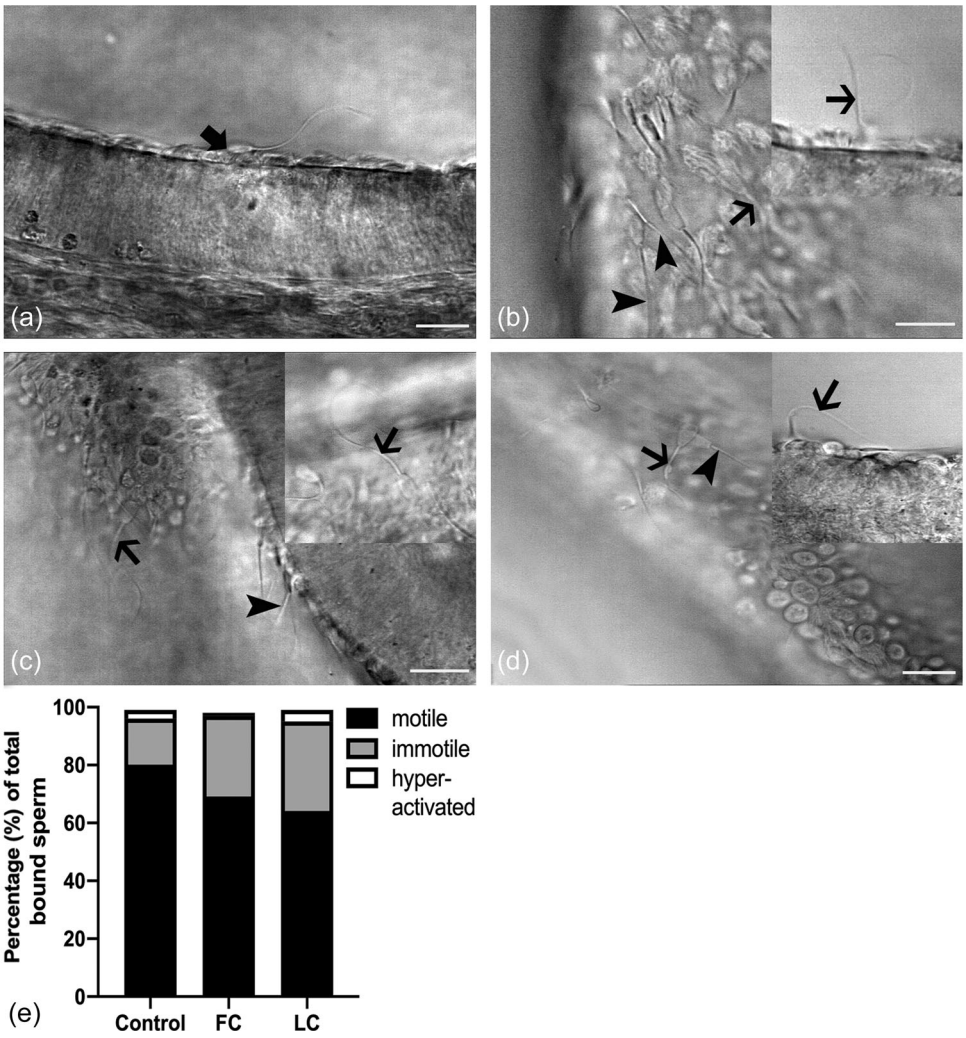

FIGURE 9 Effect of COD on the formation of the sperm reservoir and sperm motility. (a) Spermatozoa are binding at a tangential angle to the ciliated cells of the tubal epithelium both in control cows and COD cows. Sperm from (b) control, mid-diestrus cows, (c) cows with FC, and (d) cows with LC, are motile (arrows, see Movie S1), immotile (arrowheads, see Movie S1), or hyperactivated (inlay, arrow, see Movie S2). (e) There is no statistical difference in percentages of motile, immotile or hyperactivated sperm in the control ampulla from mid-diestrus cows and ampullae from cows with FC and LC ($p = 0.14$, Two-way ANOVA with Tukey's multiple comparisons test). Data are presented as mean ± *SEM*. Scale bars: 10 µm. ANOVA, analysis of variance; COD, cystic ovary disease; FC, follicular cysts; FCL, follicular cysts with luteinization.

conceals the network of oval pockets, which are pivotal for the first embryo-maternal communication (Kölle et al., 2009). Further to that, in the tubal epithelium of cows with FC, CCs are abundant and extend over the SCs with microvilli, whereas in the epithelium of cows with LC, pSCs without microvilli predominate. All these results highlight that COD exerts distinctive effects not only on the ovaries, but within the whole genital tract. Similarly, changes between ratio, relative height, and presence/absence of microvilli have also been reported during the bovine estrus cycle (Eriksen et al., 1994). This so-called remodeling in the oviductal epithelium is known to occur across the estrus cycle in many species such as the rhesus monkey (Brenner, 1969), cow (Ito et al., 2020) and bitch (Verhage et al., 1973). Thus, it might be hypothesized that the predominance of CCs in the tube of cows with FC is driven by elevated estrogen levels, whereas the abundance of SCs in LC cows might be due to high progesterone levels. In each case, our studies point to the fact that tubal epithelial cell ratios and cell morphology not only changes during the cycle, but also in the context of a reproductive disorder. Overall, the typical alterations on the inner surface of the tube, which might be visualized by optical coherence tomography (Trottmann et al., 2016), as well as the characteristic cellular patterns in the cyst aspirate might be used for the discrimination of the cyst types, thus allowing a more specific therapeutic approach. Recently, in a more macroscopic approach, current diagnostic efforts propose incorporating ultrasound and color Doppler blood flow measurements with morphological parameters such as luteal rim thickness (Turner et al., 2023). These measures might be helpful for increasing diagnostic accuracy and for reducing the dependency on synchronization treatments and the use of hormones for reproduction in livestock.

Regarding the effects of **COD on oviductal function**, one of the most interesting clinical findings is that COD cows are more likely to exhibit endometritis than the control cows. The co-existence of COD and endometritis has already been mentioned (Çolakoğlu et al., 2020; Gobikrushanth et al., 2016; Purba et al., 2021). However, to date, it remains to be elucidated whether (1) inflammation supports the development of COD by promoting the failure in the ovulation of the preovulatory follicle and preventing subsequent atresia, or whether (2) COD alters the immune response so that bacteria can more easily persist. In support of the first hypothesis, it is known that uterine infections during early postpartum affect dominant follicle growth and normal CL function (Sheldon et al., 2002; Williams et al., 2007). Similarly, Peter et al., 1989 showed that infusion of the bacterial toxin lipopolysaccharide into the uterine lumen of heifers inhibits the release of LH, which is essential for the growth of a dominant follicle into a preovulatory follicle as well as for ovulation (Peter et al., 1989). The second hypothesis based on the reduced effectiveness of the immune system, is supported by our findings that in COD cows with mild endometritis only very few immune cells are seen. To ensure that all the effects observed in COD cows were not due to endometritis we only described those results which were seen both in COD cows with and without endometritis.

The most interesting effect of COD on oviductal function for ART (assisted reproductive technologies) specialists is the alteration of the metabolic activity of the tubal epithelium. Each cyst type shows a characteristic glycoprotein and acidic mucopolysaccharide synthesis, which is highly variable as compared to the controls. The increased secretory activity of the tubal cells in cows with FC is confirmed by the results of our TEM studies which revealed abundant amounts of highly active dilated rough endoplasmic reticulum and numerous cytoplasmic SG. Increased carbohydrate synthesis has already been reported during the cycle—especially during the follicular phase (proestrus/estrus) of cycling cows (McDaniel et al., 1968), rabbits (Özen et al., 2010) and rodents (Machado-Neves et al., 2019), as well as in estrogen-treated cows (McDaniel et al., 1968)—and this has been shown both at a histochemical and ultrastructural level (Bjorkman & Fredricsson, 1961; Eriksen et al., 1994) pointing to the possibility that the alterations in FC cows are driven by the high levels of estrogen. Progesterone, on the other hand, is the dominant steroid hormone during the luteal phase (diestrus; days 10–15) and is elevated in LC cows. This hormone inhibits oviductal secretory and transport activities (Binelli et al., 2018) so that the amount of secretion and the number of SG in the oviductal cells is decreased during the luteal phase in the bovine (Abe & Oikawa, 1993; Steffl et al., 2008). The level of glycoprotein synthesis is not only altered in COD cows, but also shows a highly variable correlation coefficient. This has already been shown during inflammation of the genital tract (Owhor et al., 2019). Thus, a highly variable correlation coefficient in glycoprotein synthesis might be indicative for diseases in the genital tract.

Overall, our results demonstrate that COD alters tubal secretory patterns in a cyst-specific way which might be associated with distinctive changes in the tubal microenvironment and its subsequent ability to support the formation of the sperm reservoir, fertilization, and embryo survival and development. Regarding the formation of the sperm reservoir, which is characterized by tangential binding of the sperm head to the cilia of the oviductal cells and allows bovine sperm to maintain fertilizing capacity for 3–4 days (Kölle, 2022), we applied live cell imaging of the sperm within the oviduct to analyze whether the altered glycoprotein metabolism and the altered epithelial cells in LC cows affect motility and survival time of the sperm within the tube. Interestingly, sperm parameters were similar to sperm in control cows suggesting that—as sperm can bind all across the oviduct, both in isthmus and ampulla (Kölle, 2022)—the reduced glycoprotein synthesis in LC cows are still sufficient to maintain sperm motility and sperm survival.

Besides the altered secretory activity in the tubal cells of COD cows, TEM also reveals EM with partial loss of cristae. These findings might point to impaired oxidative phosphorylation and ATP production as well as diminished calcium storage and signal transduction in the cells. The reduced availability of energy and calcium might also contribute to the decreased transport speed as well as the diminished active epithelial ion transport seen in our previous COD studies (Scully et al., 2021). As the early embryo has to be nourished properly by the oviductal cells and has to be transported in a time-specific manner to establish a successful pregnancy, these results imply that early embryonic development in COD cows might be compromised.

Overall, our studies are the first to precisely characterize the effects of COD on the 3D microarchitecture of the inner surface, on the composition of the tubal epithelial cells as well as on glycoprotein and carbohydrate metabolism. This knowledge promotes the establishment of novel, cyst-specific therapeutic concepts in cattle and provides new ideas for the therapeutic approach of PCOS (polycystic ovarian syndrome) in humans, as ovarian morphological parameters, ovarian cellular composition, hormone cycling, mono-ovular folliculogenesis, as well as the incidence and the genetic and environmental risk factors for COD and PCOS are common between these two species (Roberts & Huang, 2022).

AUTHOR CONTRIBUTIONS

Deirdre Scully: writing—original draft; investigation; methodology; validation; visualization; writing—review & editing; software; formal analysis; project administration; data curation. **Sven Reese**: writing—review & editing; validation; formal analysis; methodology. **Sabine Kölle**: conceptualization; funding acquisition; writing—review & editing; project administration; supervision; resources.

ACKNOWLEDGMENTS

Open access funding provided by IReL.

CONFLICT OF INTEREST STATEMENT

The authors declare no conflicts of interest.

DATA AVAILABILITY STATEMENT

The data that support the findings of this study are available from the corresponding author upon reasonable request.

ORCID

Deirdre Scully https://orcid.org/0000-0002-5918-5615
Sven Reese http://orcid.org/0000-0002-4605-9791
Sabine Kölle http://orcid.org/0000-0002-4541-0498

REFERENCES

Abe, H., & Oikawa, T. (1993). Observations by scanning electron microscopy of oviductal epithelial cells from cows at follicular and luteal phases. *The Anatomical Record*, *235*(3), 399–410. https://doi.org/10.1002/ar.1092350309

Arosh, J. A., Parent, J., Chapdelaine, P., Sirois, J., & Fortier, M. A. (2002). Expression of cyclooxygenases 1 and 2 and prostaglandin E synthase in bovine endometrial tissue during the estrous cycle. *Biology of Reproduction*, *67*(1), 161–169. https://doi.org/10.1095/biolreprod67.1.161

Bastos, N. M., Ferst, J. G., Goulart, R. S., & Coelho da Silveira, J. (2022). The role of the oviduct and extracellular vesicles during early embryo development in bovine. *Animal Reproduction*, *19*(1), 1–13. https://doi.org/10.1590/1984-3143-AR2022-0015

Binelli, M., Gonella-diaza, A. M., Mesquita, F. S., & Membrive, C. (2018). Sex steroid-mediated control of oviductal function in cattle. *Biology*, *7*(15). https://doi.org/10.3390/biology7010015

Bjorkman, N., & Fredricsson, B. (1961). The bovine oviduct epithelium and its secretory process as studied with the electron microscope and histochemical tests. *Zeitschrift fur Zellforschung und mikroskopische Anatomie (Vienna, Austria: 1948)*, *55*, 500–513. https://doi.org/10.1007/BF00325415

Borş, S., & Borş, A. (2020). Ovarian cysts, an anovulatory condition in dairy cattle. *Journal of Veterinary Medical Science*, *82*(10), 1515–1522. https://doi.org/10.1292/jvms.20-0381

Brenner, R. M. (1969). Renewal of oviduct cilia during the menstrual cycle of the rhesus monkey. *Fertility and Sterility*, *20*(4), 599–611. https://doi.org/10.1016/S0015-0282(16)37086-8

Brodzki, P., Brodzki, A., Krakowski, L., Dąbrowski, R., Szczubiał, M., & Bochniarz, M. (2019). Levels of selected cytokines and acute–phase proteins in the serum of dairy cows with cystic ovarian disease and those in follicular and luteal phases of normal ovarian cycle. *Research in Veterinary Science*, *123*(December 2018), 20–25. https://doi.org/10.1016/j.rvsc.2018.12.007

Camara Pirez, M., Steele, H., Reese, S., & Kölle, S. (2020). Bovine sperm-oviduct interactions are characterized by specific sperm behaviour, ultrastructure and tubal reactions which are impacted by sex sorting. *Scientific Reports*, *10*(1), 16522. https://doi.org/10.1038/s41598-020-73592-1

Cattaneo, L., Signorini, M., Bertoli, J., Bartolomé, J., Gareis, N., Díaz, P., Bó, G., & Ortega, H. (2014). Epidemiological description of cystic ovarian disease in Argentine dairy herds: Risk factors and effects on the reproductive performance of lactating cows. *Reproduction in Domestic Animals*, *49*, 1028–1033. https://doi.org/10.1111/rda.12432

Çolakoğlu, H. E., Küplülü, S., Polat, I. M., Pekcan, M., Özenç, E., Baklacı, C., Seyrek-İntaş, K., Gümen, A., & Vural, M. R. (2020). Association among lipopolysaccharide, the transforming growth factor–beta superfamily, follicular growth, and transcription factors in spontaneous bovine ovarian cysts. *Domestic Animal Endocrinology*, *70*, 106398. https://doi.org/10.1016/j.domaniend.2019.106398

Croxatto, H. B. (2002). Physiology of gamete and embryo transport through the fallopian tube. *Reproductive BioMedicine Online*, *4*(2), 160–169. https://doi.org/10.1016/S1472-6483(10)61935-9

Dixon, R. E., Hwang, S. J., Kim, B. H., Sanders, K. M., & Ward, S. M. (2019). Myosalpinx contractions are essential for egg transport along the oviduct and are disrupted in reproductive tract diseases. *Advances in Experimental Medicine and Biology*, *1124*, 265–294. https://doi.org/10.1007/978-981-13-5895-1_11

Douthwaite, R., & Dobson, H. (2000). Comparison of different methods of diagnosis of cystic ovarian disease in cattle and an assessment of its treatment with a progesterone-releasing intravaginai device. *Veterinary Record*, *147*, 355–359. https://doi.org/10.1136/vr.147.13.355

Eriksen, T., Terkelsen, O., Hyttel, P., & Greve, T. (1994). Ultrastructural features of secretory cells in the bovine oviduct epithelium. *Anatomy and Embryology*, *190*, 583–590. https://doi.org/10.1007/BF00190108

Fernandez-Fuertes, B., Rodríguez-alonso, B., Sánchez, J. M., Simintiras, C. A., Lonergan, P., & Rizos, D. (2018). Looking at the big picture: Understanding how the oviduct' s dialogue with gametes and the embryo shapes reproductive success. *Animal Reproduction*, *15*, 751–764. https://doi.org/10.21451/1984-3143-AR2018-0036

Gareis, N. C., Rodríguez, F. M., Cattaneo Moreyra, M. L., Stassi, A. F., Angeli, E., Etchevers, L., Salvetti, N. R., Ortega, H. H., Hein, G. J., & Rey, F. (2023). Contribution of key elements of nutritional metabolism to the development of cystic ovarian disease in dairy cattle. *Theriogenology*, *197*, 209–223. https://doi.org/10.1016/j.theriogenology.2022.12.003

Ghosh, A., Syed, S. M., & Tanwar, P. S. (2017). In vivo genetic cell lineage tracing reveals that oviductal secretory cells self-renew and give rise to ciliated cells. *Development (Cambridge, England)*, *144*(17), 3031–3041. https://doi.org/10.1242/dev.149989

Ginther, O. J. (2020a). Intraovarianism. Local mechanisms that affect follicle and luteal dynamics in heifers and women. *Biology of Reproduction*, *102*(2), 265–275. https://doi.org/10.1093/biolre/ioz199

Ginther, O. J. (2020b). Selection of side of ovulation by intraovarianism in *Bos Taurus* heifers. *Biology of Reproduction*, *103*(4), 711–716. https://doi.org/10.1093/biolre/ioaa118

Gobikrushanth, M., Salehi, R., Ambrose, D. J., & Colazo, M. G. (2016). Categorization of endometritis and its association with ovarian follicular growth and ovulation, reproductive performance, dry matter intake, and milk yield in dairy cattle. *Theriogenology*, *86*(7), 1842–1849. https://doi.org/10.1016/j.theriogenology.2016.06.003

Ireland, J. J., Murphee, R. L., & Coulson, P. B. (1980). Accuracy of predicting stages of bovine estrous cycle by gross appearance of the corpus luteum. *Journal of Dairy Science*, *63*(1), 155–160. https://doi.org/10.3168/jds.S0022-0302(80)82901-8

Ito, S., Kobayashi, Y., Yamamoto, Y., Kimura, K., & Okuda, K. (2016). Remodeling of bovine oviductal epithelium by mitosis of secretory cells. *Cell and Tissue Research*, *366*, 403–410. https://doi.org/10.1007/s00441-016-2432-8

Ito, S., Yamaguchi, Y., Kubota, S., Yamamoto, Y., & Kimura, K. (2023). Immunohistochemical identification of epithelial cell types in the isthmus of bovine oviduct: Comparison with the ampulla. *Journal of Reproduction and Development*, *69*(1), 18–24. https://doi.org/10.1262/jrd.2022-104

Ito, S., Yamamoto, Y., & Kimura, K. (2020). Analysis of ciliogenesis process in the bovine oviduct based on immunohistochemical classification. *Molecular Biology Reports*, *47*(2), 1003–1012. https://doi.org/10.1007/s11033-019-05192-w

Kölle, S. (2022). Sperm-oviduct interactions: Key factors for sperm survival and maintenance of sperm fertilizing capacity. *Andrology*, *10*(5), 837–843. https://doi.org/10.1111/andr.13179

Kölle, S., Dubielzig, S., Reese, S., Wehrend, A., König, P., & Kummer, W. (2009). Ciliary transport, gamete interaction, and effects of the early embryo in the oviduct: Ex vivo analyses using a new digital videomicroscopic system in the cow. *Biology of Reproduction*, *81*(2), 267–274. https://doi.org/10.1095/biolreprod.108.073874

Kölle, S., Hughes, B., & Steele, H. (2020). Early embryo-maternal communication in the oviduct: A review. *Molecular Reproduction and Development*, *87*(6), 650–662. https://doi.org/10.1002/mrd.23352

Lüttgenau, J., Kögel, T., & Bollwein, H. (2016). Effects of GnRH or PGF2α in week 5 postpartum on the incidence of cystic ovarian follicles and persistent corpora lutea and on fertility parameters in dairy cows. *Theriogenology*, *85*(5), 904–913. https://doi.org/10.1016/j.theriogenology.2015.10.040

Machado-Neves, M., Assis, W. A., Gomes, M. G., & Oliveira, C. A. (2019). Oviduct morphology and estrogen receptors ERα and ERβ expression in captive *Chinchilla lanigera* (Hystricomorpha: Chinchillidae. *General and Comparative Endocrinology*, *273*(January), 32–39. https://doi.org/10.1016/j.ygcen.2018.03.023

McDaniel, J. W., Scalzi, H., & Black, D. L. (1968). Influence of ovarian hormones on histology and histochemistry of the bovine oviduct. *Journal of Dairy Science*, *51*(5), 754–761. https://doi.org/10.3168/jds.S0022-0302(68)87067-5

Noakes, D. E., Parkinson, T. J., & England, G. C. W. (2001). *Arthur's Veterinary Reproduction and Obstetrics* (8th ed.). Elsevier.

Ortega, H., Díaz, P., Salvetti, N., Hein, G., Marelli, B., Rodríguez, F., Stassi, A., & Rey, F. (2016). Follicular cysts: A single sign and different diseases. A view from comparative medicine. *Current Pharmaceutical Design*, *22*, 5634–5645. https://doi.org/10.2174/1381612822666160804

Owhor, L. E., Reese, S., & Kölle, S. (2019). Salpingitis impairs bovine tubal function and Sperm-Oviduct interaction. *Scientific Reports*, *9*, 10893. https://doi.org/10.1038/s41598-019-47431-x

Özen, A., Ergün, E., & Kürüm, A. (2010). Histomorphology of the oviduct epithelium in the Angora rabbit. *Turkish Journal of Veterinary Animal Science*, *34*(3), 219–226. https://doi.org/10.3906/vet-0710-39

Peter, A. (2004). An update on cystic ovarian degeneration in cattle. *Reproduction in Domestic Animals*, *39*(1), 1–7. https://doi.org/10.1046/j.0936-6768.2003.00466.x

Peter, A. T., Bosu, W. T., & DeDecker, R. J. (1989). Suppression of preovulatory luteinizing hormone surges in heifers after intrauterine infusions of *Escherichia coli* endotoxin. *American Journal of Veterinary Research*, *50*(3), 368–373.

Purba, F. Y., Suzuki, N., & Isobe, N. (2021). Association of endometritis and ovarian follicular cyst with mastitis in dairy cows. *Journal of Veterinary Medical Science*, *83*(2), 338–343. https://doi.org/10.1292/jvms.20-0652

Roberts, J. F., & Huang, C.-C. J. (2022). Bovine models for human ovarian diseases. In *Progress in Molecular Biology and Translational Science* (pp. 101–154). Elsevier. https://doi.org/10.1016/bs.pmbts.2022.02.001

Scully, D. M., Campion, D., McCartney, F., Dulohery, K., Reese, S., & Kölle, S. (2021). Cystic ovary disease impairs transport speed, smooth muscle contraction, and epithelial ion transport in the bovine oviduct. *Molecular Reproduction and Development*, *88*(8), 558–570. https://doi.org/10.1002/mrd.23521

Sheldon, I., Noakes, D., Rycroft, A., Pfeiffer, D., & Dobson, H. (2002). Influence of uterine bacterial contamination after parturition on ovarian dominant follicle selection and follicle growth and function in cattle. *Reproduction*, *123*(6), 837–845.

Steffl, M., Schweiger, M., Sugiyama, T., & Amselgruber, W. M. (2008). Review of apoptotic and non-apoptotic events in non-ciliated cells of the mammalian oviduct. *Annals of Anatomy - Anatomischer Anzeiger*, *190*(1), 46–52. https://doi.org/10.1016/j.aanat.2007.04.003

Suarez, S. S., & Pacey, A. A. (2006). Sperm transport in the female reproductive tract. *Human Reproduction Update*, *12*(1), 23–37. https://doi.org/10.1093/humupd/dmi047

Suarez, S. S. (2008). Regulation of sperm storage and movement in the mammalian oviduct. *The International Journal of Developmental Biology*, *52*(5–6), 455–462. https://doi.org/10.1387/ijdb.072527ss

Trottmann, M., Kölle, S., Leeb, R., Doering, D., Reese, S., Stief, C. G., Dulohery, K., Leavy, M., Kuznetsova, J., Homann, C., & Sroka, R. (2016). Ex vivo investigations on the potential of optical coherence tomography (OCT) as a diagnostic tool for reproductive medicine in a bovine model. *Journal of Biophotonics*, *9*(1–2), 129–137. https://doi.org/10.1002/jbio.201500009

Turner, Z. B., Lima, F. S., Conley, A. J., McNabb, B. R., Rowe, J. D., Garzon, A., Urbano, T. M., Morris, C. M., & Pereira, R. V. (2023). Cystic ovarian disease in dairy cattle: Diagnostic accuracy when using B-mode and color Doppler ultrasound. *Journal of Dairy Science*, *106*(5), 3411–3420. https://doi.org/10.3168/jds.2022-22498

Vanholder, T., Opsomer, G., & de Kruif, A. (2006). Aetiology and pathogenesis of cystic ovarian follicles in dairy cattle: A review. *Reproduction, Nutrition, Development*, *46*, 105–119. https://doi.org/10.1051/rnd

Verhage, H. C., Abel, J. H., Tietz, W. J., & Barrau, M. D. (1973). Development and maintenance of the oviductal epithelium during the estrous cycle in the bitch. *Biology of Reproduction*, *9*, 460–474. https://doi.org/10.1093/biolreprod/9.5.460

Williams, E. J., Fischer, D. P., Noakes, D. E., England, G. C. W., Rycroft, A., Dobson, H., & Sheldon, I. M. (2007). The relationship between uterine pathogen growth density and ovarian function in the postpartum dairy cow. *Theriogenology*, *68*(4), 549–559. https://doi.org/10.1016/j.theriogenology.2007.04.056

SUPPORTING INFORMATION

Additional supporting information can be found online in the Supporting Information section at the end of this article.

How to cite this article: Scully, D., Reese, S., & Kölle, S. (2024). Cystic ovary disease (COD) alters structure and function of the bovine oviduct. *Molecular Reproduction and Development*, *91*, e23725. https://doi.org/10.1002/mrd.23725